



Special Feature: Dynamics Modeling Supporting Vehicle Performance

Research Report

Effects of Unsteady Aerodynamic Loads on Vehicle Motion Performance

Mitsuyoshi Kawakami, Norikazu Sato, Osamu Murata and Kazuhiro Maeda

Report received on Aug. 29, 2016

■ABSTRACT■ The present study first focuses on the transient aerodynamic load associated with vehicle's vertical (heaving and pitching) motions. Dynamic wind-tunnel tests of a generic fastback car model, known as the Ahmed model, were conducted using a two-degree-of-freedom model shaker. The experimental results revealed that frequency-dependent gains and phase differences between the model height/angle and the aerodynamic loads were in close agreement with those predicted by large-eddy simulations (LESs). Based on these results, a full-unsteady aerodynamic load model was derived in the form of a linear transfer function in order to demonstrate the influence of the transient loads on the vehicle's dynamic behavior.

The second focus is on fluctuations in the aerodynamic load acting on a hatchback car model under steady and straight driving conditions. Surface pressure fluctuations predicted by LES indicated a negative correlation between the two sides of the rear end, which could excite lateral vibrations in the vehicle. In wind-tunnel tests using a 28% scale model, delta-winglet vortex generators (VGs) mounted on each side of the rear end provided a marked reduction in lateral load fluctuations. The VGs were then applied to an actual hatchback car and resulted in higher subjective ratings during a track test. This is a promising result that supports the hypothesis that suppression of aerodynamic load fluctuations improves vehicle motion performance.

■KEYWORDS■ Passenger Car, Dynamic Wind-tunnel Test, Large-eddy Simulation, Transient Aerodynamic Load, Aerodynamic Load Fluctuation, Vehicle Motion Performance

1. Introduction

Time-averaged aerodynamic loads are generally used for vehicle performance evaluation. However, it is seemingly essential to take into account time-dependent/unsteady aerodynamic loads in order to provide a realistic evaluation of vehicle handling, stability, and ride comfort. Unsteady aerodynamic loads acting on a passenger car driving in still air include transient loads associated with vehicle motions and fluctuating loads originating in the unsteady wake. Note that the latter loads exist even under static driving conditions.

Although transient aerodynamics has been of increasing interest to the automotive industry, most of the experimental studies to date have been conducted for pure yawing motions⁽¹⁻⁴⁾ in order to address gusty crosswind conditions. In contrast, due to the practical difficulties associated with the design of a robust model shaker system, numerical analyses have been shown

to have a significant advantage over experiments for vertical (i.e., heaving and pitching) motions.^(5,6)

On the other hand, load fluctuations have not been sufficiently investigated from the viewpoint of vehicle handling stability, although the identification of unsteady near-wake structures has been studied for many years. To the best of the authors' knowledge, the work by Sims-Williams et al.⁽⁷⁾ is the first to have revealed the existence of weakly coherent antisymmetric oscillations behind a realistic car model and to have implied their possible effect on the degradation of straight-line stability.

In the present study, dynamic wind-tunnel tests with a generic fastback car model as defined by Ahmed et al.⁽⁸⁾ were first conducted using a two-degree-of-freedom (DOF) model shaker⁽⁹⁾ for sinusoidal vertical oscillations. The frequency response of the aerodynamic loads was then compared with that predicted by large-eddy simulations (LESs).⁽¹⁰⁾ The first goal of the present study is to derive a transient

aerodynamic load model expressed in linear form and to incorporate this model into the vehicle's equation of motion in a way that allows a quick and efficient evaluation of the vehicle system response.⁽¹¹⁾

Similarly, a transient load model of a realistic hatchback car model was derived for sinusoidal lateral oscillations using a six-DOF model shaker that was recently developed in-house.⁽¹²⁾ (The results are not shown herein.) However, the effects of aerodynamic devices could not be well explained by a preliminary vehicle motion analysis for a lane change maneuver. Note that the transient load model was based on phase-averaged loads, so the fluctuating components were inherently excluded from the analysis.

Therefore, the second goal of the present study is to clarify the influence of the fluctuations in the aerodynamic loads on the handling stability.⁽¹³⁾ Large-eddy simulations and scale-model wind-tunnel tests were first performed with the hatchback car model under straight driving conditions in order to examine the aerodynamic fluctuations. The experimental results led to the concept of an effective device in terms of fluctuation reduction, the effect on vehicle motion performance of which was then subjectively evaluated on a test track.

2. Method for Studying Transient Aerodynamic Loads

2.1 Dynamic Wind-tunnel Test

Dynamic wind-tunnel tests were performed in a closed-circuit, 1:2 scale automotive wind tunnel at RUAG Aviation, Switzerland. The nozzle exit was 2.45 m wide and 1.55 m high. The test section was 3/4 open and was equipped with a moving belt system. The Ahmed model with a rear-end slant angle of 12.5° was chosen as the subject for the present study. **Figure 1** shows a perspective view of the Ahmed model equipped with the internal model shaker attached to the end of the overhead support strut. The model shaker consisted of two hydraulic actuators, which allowed two-DOF vertical motion. The overall length L and the frontal projected area A of the model were 1.044 m and 0.112 m^2 , respectively.

The transient aerodynamic forces and moments were measured with a built-in six-component balance in the shaker. The load data were sampled at 400 Hz, and the raw data were phase averaged over

36 to 144 motion cycles, depending on the motion frequency. The free-stream velocity U was set to 40 m/s, giving a Reynolds number of 2.8×10^6 based on the model length L .

2.2 Numerical Simulation

Corresponding numerical simulations were conducted using an in-house LES code for three-dimensional incompressible flows, extended to the arbitrary Lagrangian-Eulerian (ALE) coordinate system. For the modeling of sub-grid scale (SGS) components, a mixed-time-scale SGS model was used.⁽¹⁴⁾ A detailed description of the code is given in Reference (10).

The computational domain employing an overlaid grid system consisted of an inner structured grid and a background orthogonal grid. The former was transformed with the vehicle motion, whereas the latter was fixed. The number of inner grid points was $215 (L) \times 72 (W) \times 123 (H)$, and there were $123 \times 35 \times 62$ points for the background grid. Note that a half model was used in order to reduce computational cost. The minimum grid spacing adjacent to the model was 0.1 mm.

2.3 Vehicle Motion Analysis

The four-DOF half-car suspension model used in the vertical motion analysis is illustrated in **Fig. 2**, where the Ahmed model scaled up by

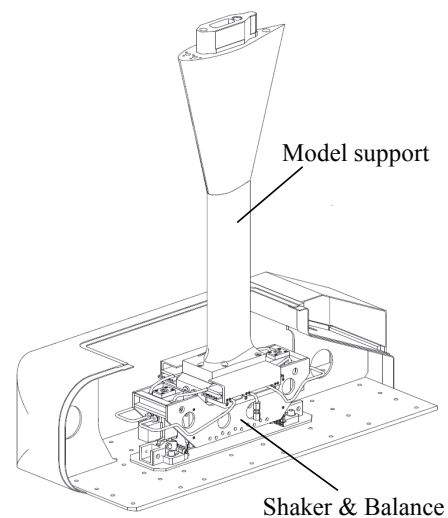


Fig. 1 Ahmed model equipped with an internal model shaker.

a factor of four is considered. Here, z_f and z_r are the vertical displacements of the front and rear wheels, respectively, and z_{f0} and z_{r0} are the excitations from the road surface of the front and rear wheels, respectively. The specifications of the suspension model are based on Kojima et al.⁽¹⁵⁾

Let the aerodynamic coefficient C (C_Z : lift coefficient, C_{MY} : pitching moment coefficient) be decomposed in the form of $C = \bar{C} + \Delta C$, where \bar{C} and ΔC represent the time-averaged component at the default position ($z = 0, \theta = 0$) and the transient component associated with the vehicle motion, respectively. The equations of motion for the vehicle body and the front/rear wheels are:

$$M\ddot{z} = -2k_f(z + l_f\theta - z_f) - 2c_f(\dot{z} + l_f\dot{\theta} - \dot{z}_f) - 2k_r(z - l_r\theta - z_r) - 2c_r(\dot{z} - l_r\dot{\theta} - \dot{z}_r) + \frac{1}{2}\rho U^2 A(\bar{C}_Z + \Delta C_Z), \quad (1)$$

$$J\ddot{\theta} = -2l_f k_f(z + l_f\theta - z_f) - 2l_f c_f(\dot{z} + l_f\dot{\theta} - \dot{z}_f) + 2l_r k_r(z - l_r\theta - z_r) + 2l_r c_r(\dot{z} - l_r\dot{\theta} - \dot{z}_r) + \frac{1}{2}\rho U^2 AL(\bar{C}_{MY} + \Delta C_{MY}), \quad (2)$$

$$m\ddot{z}_f = k_f(z + l_f\theta - z_f) + c_f(\dot{z} + l_f\dot{\theta} - \dot{z}_f) - k_t(z_f - z_{f0}), \quad (3)$$

$$m\ddot{z}_r = k_r(z - l_r\theta - z_r) + c_r(\dot{z} - l_r\dot{\theta} - \dot{z}_r) - k_t(z_r - z_{r0}). \quad (4)$$

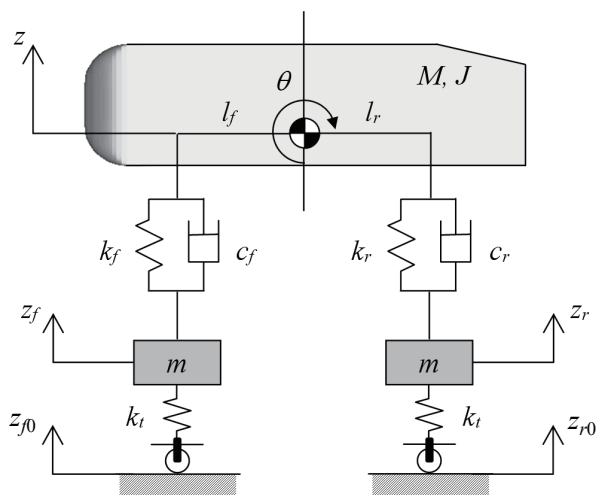


Fig. 2 Half-car suspension model with four degrees of freedom.

3. Method for Studying Aerodynamic Load Fluctuations

3.1 Numerical Simulation

The subject of the present study was a simplified hatchback car model based on a production vehicle. The overall length L and the frontal projected area A were 4.226 m and 2.126 m², respectively.

Numerical simulations were performed under straight driving conditions using the previously described LES code with an overlaid grid system. The number of inner grid points was 293 (L) × 179 (W) × 162 (H), and the background grid had 80 × 69 × 45 points. The minimum grid spacing adjacent to the model was 1 mm. The free-stream velocity U was set to 33.3 m/s, giving a Reynolds number of 9.38×10^6 based on the model length L . A velocity boundary condition equal to U was imposed on the ground plane, and wheel rotation was expressed by the angular velocity boundary condition.

For the LES analysis, three configurations were considered: the baseline model and two modified models equipped with different aerodynamic devices that had received good subjective assessments by drivers, as depicted in **Figs. 3(a)** and **(b)**. One device was a roof-side spoiler, which was designed to extend

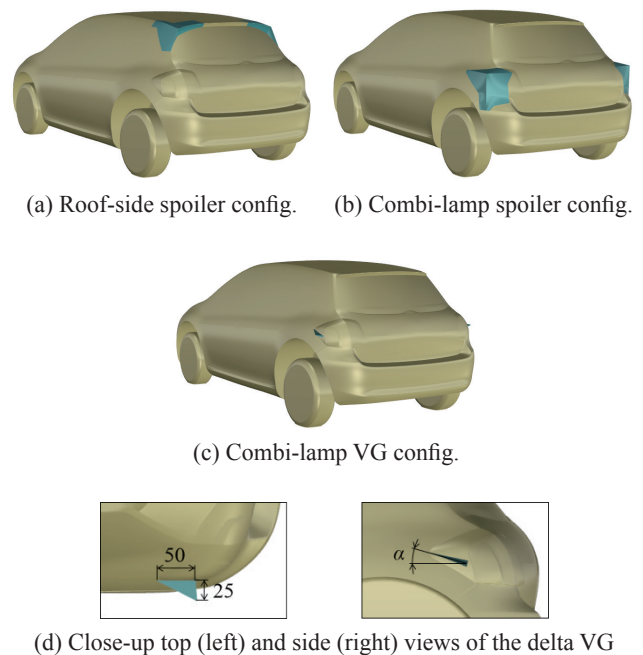


Fig. 3 Modified hatchback car models with aerodynamic devices highlighted in blue.

the rear roof spoiler from its side end to the upper rear pillar, and the other device was a combi-lamp spoiler, which changed the shape around the rear combination lamp to provide a sharply angulated corner.

3.2 Scale Model Wind-tunnel Test

Wind-tunnel tests were conducted with the 28% scale hatchback car model in a closed-circuit, 1:4 scale automotive wind tunnel at Toyota Central R&D Labs., Inc., Japan. The nozzle exit was 1.6 m wide and 1.2 m high. The test section was 3/4 open and was equipped with a fixed floor. The car body was supported from above by a vertical strut, while stationary wheels were fixed to the floor separately from the body.

The fluctuating pressure at selected points on the sides of the rear end was measured using miniature piezoresistive pressure transducers. Each transducer was connected to a pressure tap inside the model via short tubes. On the other hand, the fluctuating aerodynamic forces and moments were measured using a six-component balance mounted inside the model. The pressure and load data were recorded at a sampling rate of 500 Hz.

For the load measurements, two additional configurations were considered. The combined spoiler configuration (not shown) was a simple combination of the roof-side and combi-lamp spoiler configurations. The combi-lamp vortex generator (VG) configuration featured a delta-winglet VG mounted on the rear combination lamp, as depicted in Figs. 3(c) and (d). The length and height of the delta VG were 50 mm and 25 mm, respectively, and the attack angle α was 15° .

A wake survey was conducted for the baseline and combi-lamp VG configurations using hot-wire anemometry. The nominal streamwise velocity data were sampled at 800 Hz. During the hot-wire measurements, the load data were simultaneously recorded to allow for a cross-correlation analysis, and the sampling rate was set to be identical to that for the velocity data. The free-stream velocity U was set to 40 m/s, which yields a Reynolds number of 3.15×10^6 based on the model length of 1.183 m.

3.3 On-track Subjective Evaluation

A subjective evaluation was performed by four experienced drivers with the actual production vehicle with and without the delta VG on a 5-km-long oval test

track at the Shibetsu Proving Ground of Toyota Motor Corporation. The length and height of the combi-lamp VG used for the full-scale vehicle were 140 mm and 50 mm, respectively. The VG angle of attack of 15° was identical to that used in the wind-tunnel test. The vehicle speed was maintained at 120 km/h.

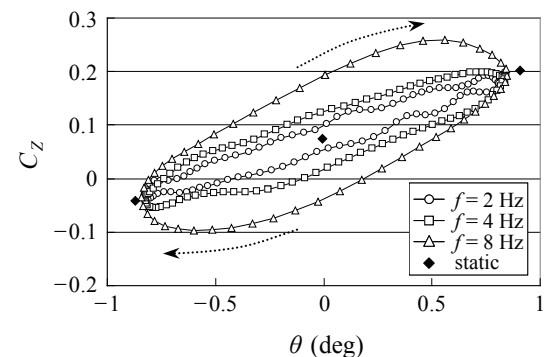
4. Results and Discussion

4.1 Transient Aerodynamic Loads

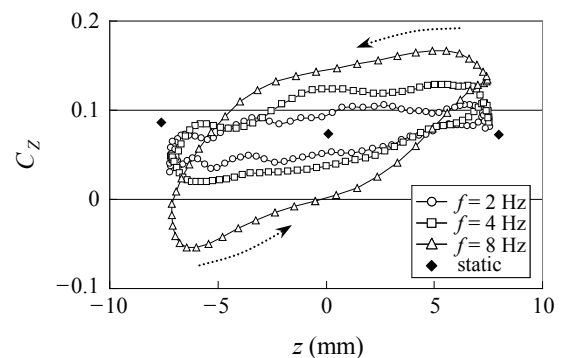
In this section, a transient aerodynamic load model is derived in order to demonstrate the influence of the transient loads on the vehicle's dynamic behavior when subjected to road excitation.

4.1.1 Frequency Response Characteristics

Figure 4 illustrates the phase-averaged Lissajous curves for the lift coefficient C_z determined from the dynamic wind-tunnel tests for the Ahmed model subjected to a pitching motion with an amplitude of 0.878° and to a heaving motion with an amplitude



(a) Pitching motions with $\theta_{\max} = 0.878^\circ$



(b) Heaving motions with $z_{\max} = 8$ mm

Fig. 4 Lissajous curves for the lift coefficients for sinusoidal vertical motions of the Ahmed model.

of 8 mm. The forcing frequencies were set to 2 Hz, 4 Hz, and 8 Hz. Also plotted in the figure are the lift coefficients measured under static conditions (corresponding to a forcing frequency of 0 Hz). Note that the moving belt system was not activated.

As shown in Fig. 4(a), the lift coefficients plotted against the pitch angle form loops, indicating the presence of a phase shift, and moreover, the amplitudes of the lift coefficients tend to increase with increasing forcing frequency. Here, the Lissajous curves for the lift coefficient rotate clockwise (as indicated by the dotted arrow), meaning that the lift coefficient is phase leading the model angle.

The lift coefficients plotted against the model height in Fig. 4(b) display essentially the same tendency, except that the slope of the Lissajous curve steepens with increasing frequency. The rotational directions for the Lissajous curves are counterclockwise, indicating a phase lag.

Assuming a linear system, the relationship between the input (normalized model height and pitch angle: z/L , θ) and output (transient components of the aerodynamic coefficients: ΔC_Z , ΔC_{MY}) signals is expressed in the following equation, which introduces the transfer function matrix G :

$$\begin{bmatrix} \Delta C_Z \\ \Delta C_{MY} \end{bmatrix} = \begin{bmatrix} G_{11} & G_{12} \\ G_{21} & G_{22} \end{bmatrix} \begin{bmatrix} z/L \\ \theta \end{bmatrix}. \quad (5)$$

The transfer function for the well-known quasi-unsteady aerodynamic model⁽¹⁶⁾ is formulated in the following equations, in which the effect of the motion rates is taken into account as an equivalent change in the relative inflow angle:

$$G_{11} = -\frac{L}{U} \left(\frac{\partial C_Z}{\partial \theta} + \bar{C}_x \right) s + \frac{\partial C_Z}{\partial(z/L)}, \quad (6)$$

$$G_{12} = -\frac{R_{12}^* L}{U} \left(\frac{\partial C_Z}{\partial \theta} + \bar{C}_x \right) s + \frac{\partial C_Z}{\partial \theta}, \quad (7)$$

$$G_{21} = -\frac{L}{U} \frac{\partial C_{MY}}{\partial \theta} s + \frac{\partial C_{MY}}{\partial(z/L)}, \quad (8)$$

$$G_{22} = -\frac{R_{22}^* L}{U} \frac{\partial C_{MY}}{\partial \theta} s + \frac{\partial C_{MY}}{\partial \theta}, \quad (9)$$

where C_x is the drag coefficient, and s is the Laplace operator. Moreover, R^* is defined as R/L , where R

denotes a characteristic radius that provides the motion rate for the pitching motions. In a previous study,⁽¹⁷⁾ R was treated as a geometric dimension. However, in the present study, assuming R is a parameter related to the vehicle's shape and motion type, R_{12}^* and R_{22}^* in Eqs. (7) and (9) are estimated by least-squares fitting to the numerically obtained time waveforms of C_Z and C_{MY} , respectively, for a pitching motion of $f = 8$ Hz and $\theta_{\max} = 0.878^\circ$.

Substituting $s = j\omega$ ($\omega = 2\pi f$) into Eqs. (6) and (7), the gain $|G(j\omega)|$ and phase $\angle G(j\omega)$ for C_Z in heaving and pitching motions are given by Eqs. (10) and (11) and Eqs. (12) and (13), respectively, which indicate that the gain increases with increasing non-dimensional frequency f^* (defined as fL/U), while the phase approaches a 90° lag for the heaving motion and either a 90° lag or a 90° lead for the pitching motion, depending on the sign of R^* .

$$|G_{11}(j\omega)| = \sqrt{\left(\frac{\partial C_Z}{\partial(z/L)} \right)^2 + \left[2\pi f^* \left(\frac{\partial C_Z}{\partial \theta} + \bar{C}_x \right) \right]^2}, \quad (10)$$

$$\angle G_{11}(j\omega) = \tan^{-1} \left[-\frac{2\pi f^* \left(\frac{\partial C_Z}{\partial \theta} + \bar{C}_x \right)}{\partial C_Z / \partial(z/L)} \right], \quad (11)$$

$$|G_{12}(j\omega)| = \sqrt{\left(\frac{\partial C_Z}{\partial \theta} \right)^2 + \left[2\pi f^* R_{12}^* \left(\frac{\partial C_Z}{\partial \theta} + \bar{C}_x \right) \right]^2}, \quad (12)$$

$$\angle G_{12}(j\omega) = \tan^{-1} \left[-\frac{2\pi f^* R_{12}^* \left(\frac{\partial C_Z}{\partial \theta} + \bar{C}_x \right)}{\partial C_Z / \partial \theta} \right]. \quad (13)$$

Figures 5 and 6 show the frequency response of C_Z , where the experimental and numerical results are plotted for different conditions (such as different motion amplitudes and free-stream velocities, with and without the activation of the moving belt). The gain and phase were estimated by least-squares fitting a sine wave to the time waveforms of both the model height/angle and the lift coefficients. In these figures, the gain and phase curves predicted by the quasi-unsteady aerodynamic model (denoted by QUM) are also plotted as solid lines.

As shown in Fig. 5, the gain and phase of C_Z for

pitching motions fall upon a single curve when plotted against the non-dimensional forcing frequency f^* , and are consistent with the quasi-unsteady model. On the other hand, it can be clearly seen from Fig. 6 that the phase response of C_z for heaving motions departs from the quasi-unsteady model in the range of f^* higher than approximately 0.1. This discrepancy is readily understood as the contribution from the added mass that is inherently involved in the numerical results and is taken into account in the experimental results but is not considered in the quasi-unsteady model.

Based on the above discussion, the added mass term was integrated into the quasi-unsteady model to derive a full-unsteady model. Equation (6) is rewritten as follows:

$$G_{11} = -\frac{2c_m VL}{U^2 A} s^2 - \frac{L}{U} \left(\frac{\partial C_z}{\partial \theta} + \bar{C}_x \right) s + \frac{\partial C_z}{\partial(z/L)}, \quad (14)$$

where V is the volume of the vehicle model.

The added mass coefficient, denoted by c_m , was estimated by least-squares fitting. The identified c_m value of 1.787 is of the same order as the theoretically estimated value of 1.5 under the assumption of a two-dimensional potential flow.

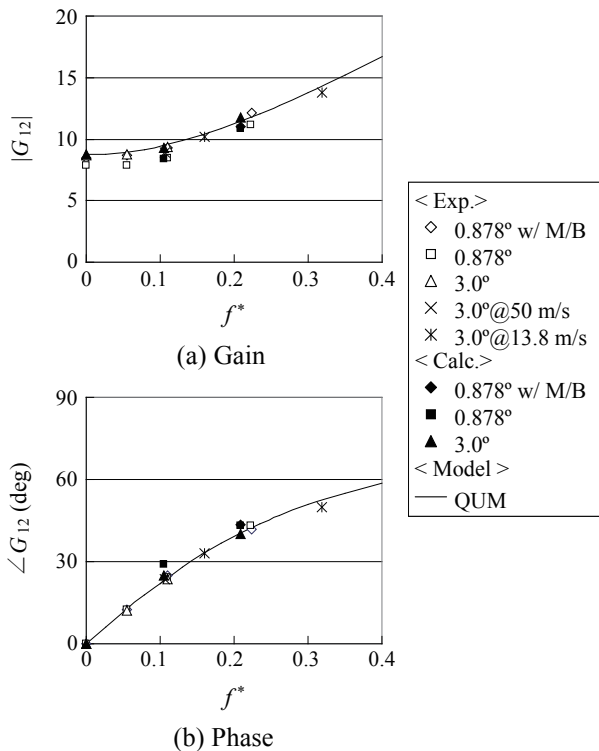


Fig. 5 Frequency response of C_z for sinusoidal pitching motions of the Ahmed model ($R_{12}^* = -0.630$).

In Fig. 6, the gain and phase curves predicted by the full-unsteady aerodynamic model (denoted by FUM) are plotted as dashed lines. It is clearly seen that the frequency response of C_z for heaving motion is successfully reproduced using the full-unsteady model.

In the same manner, the full-unsteady aerodynamic model for C_{MY} for pitching motions is derived as follows:

$$G_{22} = -\frac{2c_j \int (x^2 + z^2) dV}{U^2 AL} s^2 - \frac{R_{22}^* L}{U} \frac{\partial C_{MY}}{\partial \theta} s + \frac{\partial C_{MY}}{\partial \theta}, \quad (15)$$

where the added moment-of-inertia coefficient c_j was estimated to be 0.608.

4. 1. 2 Vehicle Motion Analysis

Figure 7 shows the result of the vehicle dynamic simulation, where the frequency response of the vertical displacement z of the sprung mass to a sinusoidal road surface input z_0 is plotted for four different aerodynamic models, A through D. Model A takes into account only the time-averaged component

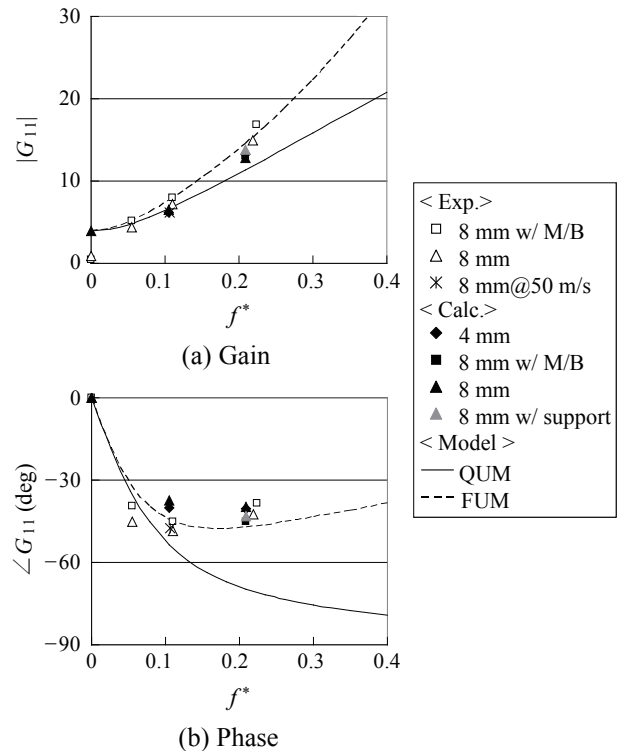


Fig. 6 Frequency response of C_z for sinusoidal heaving motions of the Ahmed model.

at the default position, and in models B through D, the displacement-dependent (aerodynamic stiffness), velocity-dependent (aerodynamic damping), and acceleration-dependent (added mass) terms are sequentially appended to model A, which yields the full-unsteady model.

It appears that the transient aerodynamic loads affect the frequency response in such a way as to reduce the resonance frequency of the sprung mass, which is caused by the reduced stiffness of the system due to the negative aerodynamic stiffness, as reported previously.⁽¹⁵⁾ Moreover, it is obvious that the acceleration-dependent term has little impact on the vehicle dynamics. Although it may seem paradoxical, the added mass term, which appears to have the effect of causing the negative aerodynamic stiffness to increase with increasing frequency (as shown in Fig. 4), should therefore be correctly described as an acceleration-dependent term. Otherwise, transient aerodynamic effects might be overestimated in the vehicle dynamic analyses.

4.2 Aerodynamic Load Fluctuations

In this section, the fluctuation in the aerodynamic loads (in particular, the lateral load) is discussed in order to verify the hypothesis that fluctuations in the aerodynamic load lead to a reduction in vehicle stability due to excitation of vehicle vibration.

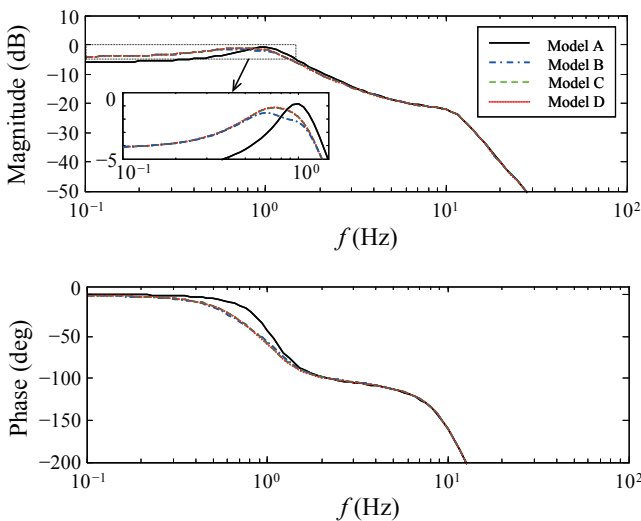


Fig. 7 Frequency response of the vertical displacement z to the road surface input z_{r0} .

4.2.1 Unsteady Near-wake Structures (Numerical Results)

Figure 8 shows power spectral density (PSD) estimates for the aerodynamic rolling and yawing moments acting on the baseline, roof-side spoiler, and combi-lamp spoiler models with the horizontal axis showing the Strouhal number (St) based on the free-stream velocity and the square root of the model frontal area. Each spectrum is the average of only three periodograms, and hence the reliability of the spectral peaks is not very high. Nevertheless, it can be seen that the spectral magnitudes are reduced relative to the baseline model in the Strouhal number range of approximately 0.05 to 0.1 for the roof-side spoiler model, and for less than 0.1 for the combi-lamp spoiler model.

Figure 9 illustrates the model surface distributions of $(C_p)_{rms}$, defined as the root-mean-square (rms) values of the static pressure coefficient fluctuations filtered from 0 to 1.0 Hz ($St = 0-0.044$) on the left and 1.0 to 2.15 Hz ($St = 0.044-0.094$) on the right, for the frequency ranges in which noticeable differences in PSD values were observed. As can be clearly seen, most of the pressure fluctuations in both frequency bands

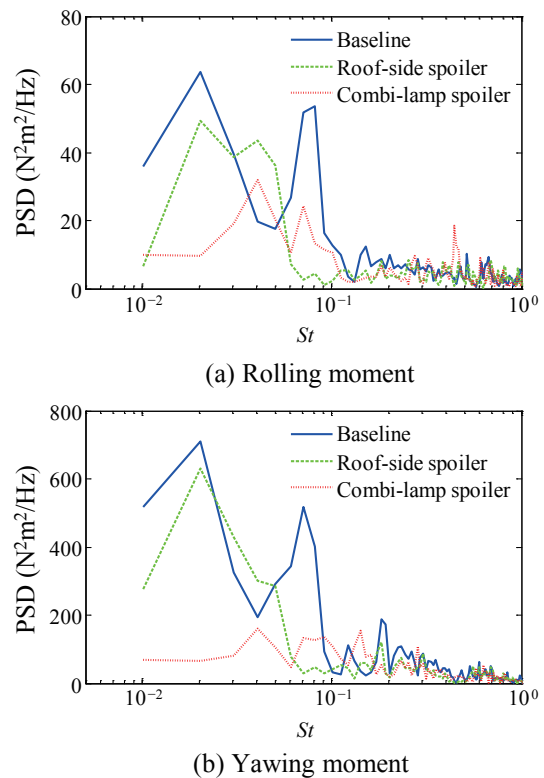


Fig. 8 Power spectral density estimates of the aerodynamic moments acting on the hatchback car models.

arise locally in the expected vicinity of flow separation at the rear end. The roof-side spoiler contributes considerably to the reduced pressure fluctuations at the roof end and the rear pillars. Although the figures are not shown, the $(C_p)_{rms}$ distribution for the combi-lamp spoiler model remained almost unchanged from that for the baseline model.

To gain further insight into the near-wake structures, the cross-correlation functions were calculated using static pressure signals at pairs of symmetric points, labeled L1 and R1, as shown in Fig. 10. The pressure

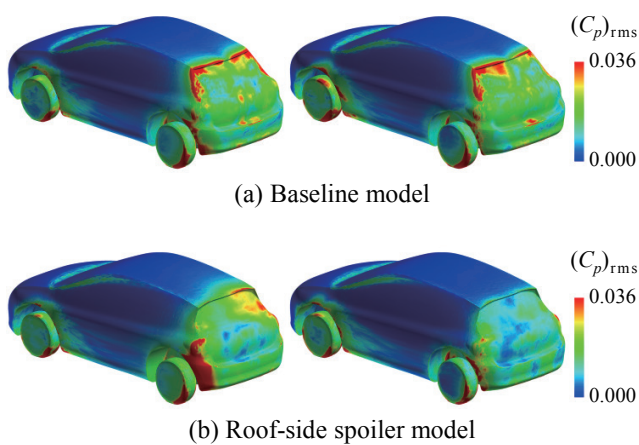


Fig. 9 Distributions of the rms values of the static pressure coefficient fluctuations on the hatchback car models (left: $(C_p)_{rms}$ filtered from 0 to 1.0 Hz; right: $(C_p)_{rms}$ filtered from 1.0 to 2.15 Hz).

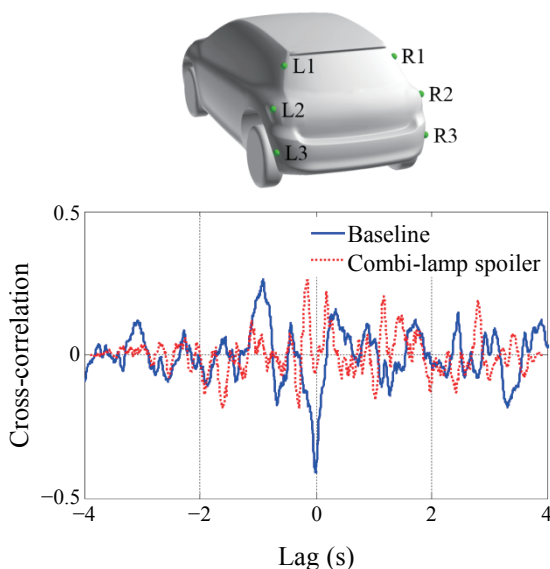


Fig. 10 Cross-correlation functions for the static pressure signals at the symmetric points labeled L1 and R1 as shown at the top of the figure.

fluctuations at the rear pillars of the baseline model demonstrate a negative correlation between the two opposite sides of the model, whereas this is not the case for the combi-lamp spoiler model. It is postulated that this negative correlation is responsible for the yawing and rolling moment fluctuations. In-phase pressure fluctuations at two sides of the model (if any) cancel each other out, and so do not contribute to the yawing and rolling moments.

4. 2. 2 Unsteady Near-wake Structures (Experimental Results)

In contrast to the LES results, a negative pressure correlation was experimentally observed at the rear combination lamps (not at the rear pillars) for the 28% scale baseline model (data not shown). At this time, a clear explanation has not yet been established for the discrepancy between the experimental and numerical results. However, based on the experimental findings, a delta-winglet VG, which has been widely adopted as a separation control device, was installed at the location where the negative correlation existed (i.e., rear combination lamp), in an attempt to reduce the aerodynamic load fluctuations.

Figure 11 shows PSD estimates for the aerodynamic rolling and yawing moments acting on the hatchback car models. The steep increase in the spectral magnitude at approximately $St = 0.1$ seen in Fig. 11(a) is due to the occurrence of resonance in the load measurement system at 11.7 Hz; otherwise, no distinct peak is observed.

As expected, the roof-side spoiler and combi-lamp spoiler models exhibit reduced spectral magnitudes for $St < 0.02-0.03$, although the Strouhal number range is not consistent with the result ($St < 0.1$) for the full-scale simulation. Moreover, the combi-lamp VG model achieves a further reduction in the spectrum magnitudes, such that the spectra are almost equivalent to those for the combined spoiler model. Note that the combi-lamp VG had little influence on the time-averaged drag, lift, and pitching moment (data not shown), so a pure assessment of the aerodynamic load fluctuations would be expected on track tests.

Figures 12 and 13 illustrate the results obtained from the wake survey using hot-wire anemometry on the yz -plane at a position 21 mm downstream of the model, and on the xy -plane at a position 250 mm above the test section floor, respectively, for the baseline

model to the left and the combi-lamp VG model to the right.

Figure 12 shows contour plots of the turbulence intensity u_{rms} , defined as the rms value of the hot-wire effective velocity fluctuations filtered between 0 and 2.0 Hz ($St = 0-0.02$), expressed as a percentage of the free-stream velocity U . The low-frequency fluctuation of interest is predominantly concentrated

in the vicinity of the rear combination lamp behind the baseline model. When the VG is in place, the peak is considerably weakened.

Figure 13 illustrates contour plots of the cross-correlation coefficients between the yawing moment and the hot-wire effective velocity throughout the measurement plane, where both signals were digitally low-pass filtered at 8.6 Hz ($St \sim 0.088$) below

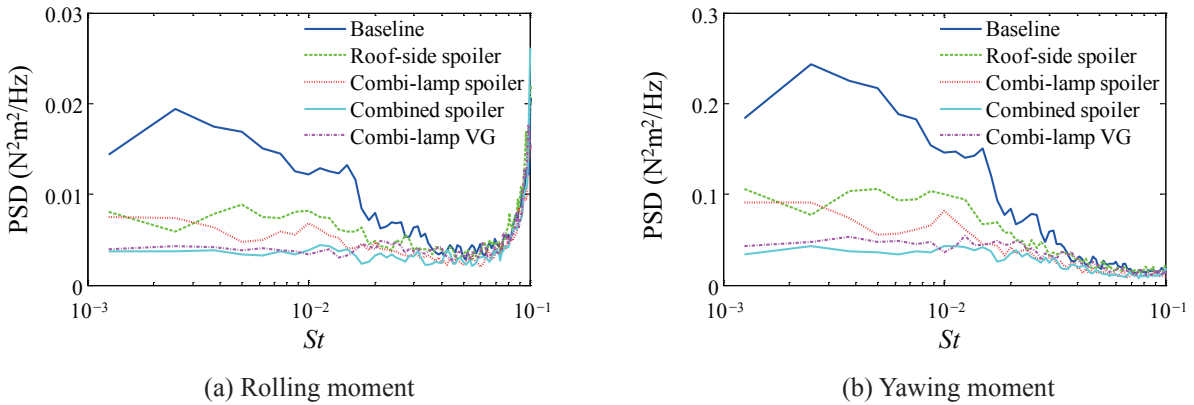


Fig. 11 PSD estimates of the aerodynamic moments acting on the 28% scale hatchback car models.

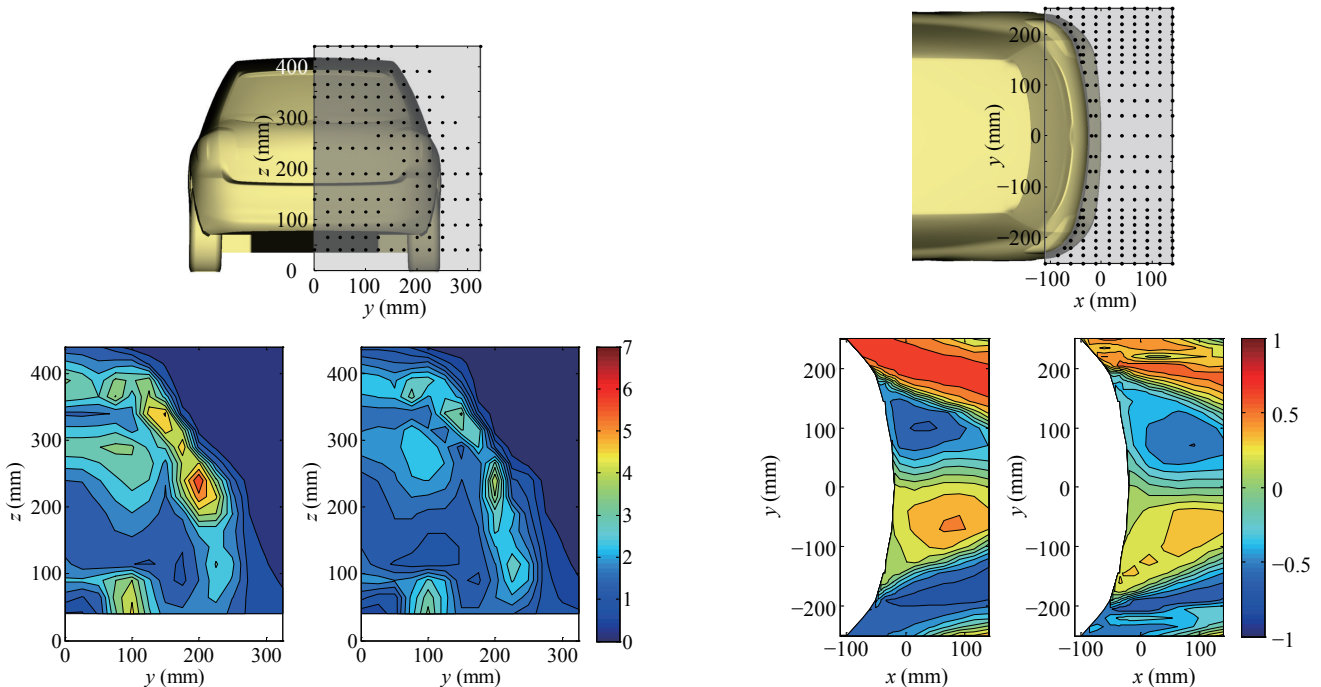


Fig. 12 Contour plots of the rms values of the hot-wire effective velocity fluctuations filtered between 0 and 2.0 Hz on the yz -plane at a position 21 mm downstream of the hatchback car model, as shown at the top of the figure (left: baseline model; right: combi-lamp VG model).

Fig. 13 Contour plots of the cross-correlation coefficients between the yawing moment and hot-wire effective velocity fluctuations on the xy -plane at a position 250 mm above the test section floor behind the hatchback car model, as shown at the top of the figure (left: baseline model; right: combi-lamp VG model).

the resonance frequency prior to the correlation analysis. It is obvious that the two sides of the wake are nearly antisymmetric; i.e., when the shear flow from the right side of the model increases in velocity, that from the left side decreases, which together induce a yawing moment in the positive direction. The reversal of the sign of the correlation for the asymmetric structure in between is probably due to inverted velocity signals from the hot-wire in reverse flow.

The correlation coefficients at the separated shear layers are slightly lowered by the VGs, but the antisymmetric structure is still prominent. The combi-lamp VG configuration was originally intended to break the side-to-side correlation by a VG-induced three-dimensionality of the separated shear layers. However, it turned out that the reduced moment fluctuations were mainly due to the reduction in the velocity fluctuations and hence the pressure fluctuations themselves.

4. 2. 3 Subjective Evaluation by Drivers

Subjective evaluations were performed by drivers focusing mainly on the vehicle performance around the neutral/on-center region, which is seemingly directly associated with low-frequency vehicle vibrations.

With the combi-lamp VG configuration, the straight line stability, steering effort around the neutral position, yaw response, and linearity were subjectively evaluated as being improved relative to the baseline configuration. The first two assessments are readily understood to be affected by yawing and rolling moment fluctuations. On the other hand, their effects on vehicle motion may not be straightforward; it is nevertheless plausible to assume that the improved initial steering response has a beneficial effect on subsequent vehicle motion through a closed-loop steering action by the driver.

5. Conclusions

The first goal of the present study was to derive a transient aerodynamic load model to be coupled with a vehicle dynamic simulation. For that purpose, dynamic wind-tunnel tests and LESs were performed on the Ahmed model in vertical motions.

Transient aerodynamic loads were then successfully depicted in linear form, extending the quasi-unsteady model (with a minor interpretational modification to

the characteristic radius R) by taking into account the added mass and moment-of-inertia effects. Although the acceleration-dependent terms were eventually confirmed to have little effect on the vehicle dynamics, they were found to be essential in order to correctly model the transient aerodynamic loads.

The second goal was to reveal the impact of the aerodynamic load fluctuations on the vehicle handling stability. To that end, LESs and scale-model wind-tunnel tests were conducted on a hatchback car model based on a production vehicle under steady straight driving conditions.

The numerically predicted surface pressure signals on the baseline model indicated a negative correlation between both rear pillars, which could give rise to yawing and rolling vibrations. On the other hand, in the wind-tunnel tests, anti-phase fluctuations were observed between both of the rear combination lamps. Although the cause of the discrepancy remains unclear, the delta-winglet VG positioned at the combination lamps led to a marked reduction in yawing and rolling moment fluctuations.

The delta VGs were then applied to an actual hatchback car and resulted in better subjective assessments of initial responses to steering inputs on a track test. This is a promising result that supports the hypothesis that suppression of aerodynamic load fluctuations improves the vehicle motion performance.

Acknowledgements

The authors would like to thank Dr. P. Aschwanen and Dr. J. Müller from RUAG Aviation for productive discussions about certain aspects of this paper. The numerical simulations were performed on the Earth Simulator at the Japan Agency for Marine-Earth Science and Technology.

References

- (1) Garry, K. P. and Cooper, K. R., "Comparison of Quasi-static and Dynamic Wind Tunnel Measurements on Simplified Tractor-trailer Models", *J. Wind Eng. Ind. Aerodyn.*, Vol. 22 (1986), pp. 185-194.
- (2) Passmore, M. A. and Mansor, S., "The Measurement of Transient Aerodynamics Using an Oscillating Model Facility", *SAE Tech. Pap. Ser.*, No. 2006-01-0338 (2006).
- (3) Mansor, S. and Passmore, M. A., "Estimation of Bluff Body Transient Aerodynamics Using an Oscillating Model Rig", *J. Wind Eng. Ind. Aerodyn.*, Vol. 96

- (2008), pp. 1218-1231.
- (4) Guilmineau, E. and Chometon, F., “Numerical and Experimental Analysis of Unsteady Separated Flow behind an Oscillating Car Model”, *SAE Int. J. Passeng. Cars – Mech. Syst.*, Vol. 1, No. 1 (2009), pp. 646-657.
- (5) Nakashima, T. et al., “Flow Structures above the Trunk Deck of Sedan-type Vehicles and Their Influence on High-speed Vehicle Stability – 2nd Report: Numerical Investigation on Simplified Vehicle Models Using Large-eddy Simulation”, *SAE Int. J. Passeng. Cars – Mech. Syst.*, Vol. 2, No. 1 (2009), pp. 157-167.
- (6) Tsubokura, M. et al., “Development of an Unsteady Aerodynamic Simulator Using Large-eddy Simulation Based on High-performance Computing Technique”, *SAE Int. J. Passeng. Cars – Mech. Syst.*, Vol. 2, No. 1 (2009), pp. 168-178.
- (7) Sims-Williams, D., Dominy, R. and Howell, J., “An Investigation into Large Scale Unsteady Structures in the Wake of Real and Idealized Hatchback Car Models”, *SAE Tech. Pap. Ser.*, No. 2001-01-1041 (2001).
- (8) Ahmed, S. R., Ramm, G. and Faltin, G., “Some Salient Features of the Time-averaged Ground Vehicle Wake”, *SAE Tech. Pap. Ser.*, No. 840300 (1984).
- (9) Aschwanden, P., Müller, J. and Knörnschild, U., “Experimental Study on the Influence of Model Motion on the Aerodynamic Performance of a Race Car”, *SAE Tech. Pap. Ser.*, No. 2006-01-0803 (2006).
- (10) Sato, N. et al., “LES Analysis of Flows around a Simplified Car Model in Vertical Motions”, *Proc. 8th Int. Symp. on Eng. Turb. Modeling Meas.*, No. 2 (2010), pp. 424-429.
- (11) Kawakami, M. et al., “Validation and Modeling of Transient Aerodynamic Loads Acting on a Simplified Passenger Car Model in Sinusoidal Motion”, *SAE Int. J. Passeng. Cars – Mech. Syst.*, Vol. 5, No. 1 (2012), pp. 324-339.
- (12) Kuroyanagi, H. et al., “25% Scale Automotive Wind Tunnel with a 6-DOF High Response Model Shaker”, *Proc. JSAE Ann. Congr.* (in Japanese), No. 107-12 (2012), pp. 13-16.
- (13) Kawakami, M., Murata, O. and Maeda, K., “Improvement in Vehicle Motion Performance by Suppression of Aerodynamic Load Fluctuations”, *SAE Int. J. Passeng. Cars - Mech. Syst.*, Vol. 8, No. 1 (2015), pp. 205-216.
- (14) Inagaki, M., Kondoh, T. and Nagano, Y., “A Mixed-time-scale SGS Model with Fixed Model-parameters for Practical LES”, *Trans. ASME, J. Fluids Eng.*, Vol. 127, No. 1 (2005), pp. 1-13.
- (15) Kojima, Y., Ohta, H. and Murata, O., “Effects of Aerodynamics on the Longitudinal Motion of a High-speed Vehicle – 2nd Report, Simulation Studies Using a Four-degree-of-freedom Model”, *Trans. JSME, Ser. C* (in Japanese), Vol. 61, No. 586 (1995), pp. 2307-2311.
- (16) Blevins, R. D. and Iwan, W. D., “The Galloping Response of a Two-degree-of-freedom System”, *Trans. ASME, J. Appl. Mech.*, Vol. 41, No. 4 (1974), pp. 1113-1118.
- (17) Kojima, Y., Ohta, H. and Murata, O., “Effects of Aerodynamics on the Longitudinal Motion of a High-speed Vehicle – 1st Report, Formulations of the Aerodynamic Characteristics”, *Trans. JSME, Ser. C* (in Japanese), Vol. 60, No. 579 (1994), pp. 3822-3828.

Figs. 1 and 4-6

Reprinted from *Trans. JSME* (in Japanese), Vol. 76, No. 768 (2010), pp. 2006-2015, Kawakami, M. et al., A Modeling of Unsteady Aerodynamic Forces Based on the Aerodynamic Analyses around a Simplified Car Model in Periodic Motions, © 2010 JSME.

Figs. 2 and 7

Reprinted from *SAE Int. J. Passeng. Cars – Mech. Syst.*, Vol. 5, No. 1 (2012), pp. 324-339, Kawakami, M. et al., Validation and Modeling of Transient Aerodynamic Loads Acting on a Simplified Passenger Car Model in Sinusoidal Motion, © 2012 SAE International, with permission from SAE International.

Figs. 3 and 8-13

Reprinted from *SAE Int. J. Passeng. Cars – Mech. Syst.*, Vol. 8, No. 1 (2015), pp. 205-216, Kawakami, M. et al., Improvement in Vehicle Motion Performance by Suppression of Aerodynamic Load Fluctuations, © 2015 SAE International, with permission from SAE International.

Mitsuyoshi Kawakami

Research Field:

- Vehicle Aerodynamics

Academic Degree: Ph.D.

Academic Society:

- The Japan Society of Mechanical Engineers



Norikazu Sato

Research Fields:

- Computational Fluid Dynamics
- Thermal Engineering
- Polymer Processing Simulation

Academic Degree: Ph.D.

Academic Society:

- The Japan Society of Mechanical Engineers

Award:

- JSME Medal for Outstanding Paper, 2015



Osamu Murata

Research Field:

- Wind Tunnel Testing



Kazuhiro Maeda*

Research Field:

- Vehicle Aerodynamics

Academic Societies:

- The Japan Society of Mechanical Engineers
- The Visualization Society of Japan
- Society of Automotive Engineers of Japan



* Toyota Motor Corporation